JOURNAL OF GEOPHYSICAL RESEARCH, VOL. 99, NO. D3, PAGES 5433–5447, MARCH 20, 1994

Coherent variations of monthly mean total ozone and lower stratospheric temperature

William J. Randel and Janel B. Cobb
National Center for Atmospheric Research, Boulder, Colorado

Abstract. Space-time patterns of correlation between total ozone and lower stratospheric temperature are documented, based on 14 years (1979-1992) of global monthly mean observations. Data are obtained from the total ozone mapping spectrometer (TOMS) and microwave sounding unit (MSU) channel 4, the latter being a weighted mean temperature of the 150- to 50-mbar layer. These data are analyzed (separately) for linear trend, solar cycle, quasi-biennial oscillation (QBO), and El Niño-Southern Oscillation (ENSO) variations via linear regression: significant signals are identified for each term, and the corresponding structures in ozone and temperature are found to be highly coherent. The temperature trends derived here show significant cooling of the lower stratosphere over Northern Hemisphere (NH) midlatitudes in winter-spring and over Antartica in Southern Hemisphere (SH) spring; the overall space-time patterns are similar to those determined for ozone trends. Interestingly, temperatures do not decrease over SH midlatitudes during midwinter, in spite of large ozone losses. These data furthermore show globally coherent ozone and temperature perturbations associated with both QBO and ENSO variations; a new result here shows large total ozone anomalies in middle-to-high latitudes of both hemispheres associated with ENSO events. Residuals from the ozone and temperature time series (defined as the deseasonalized total minus the regression fits) show strong positive correlation in middle-to-high latitudes but weak correlations in the tropics. Time periods following the volcanic eruptions of El Chichon and Pinatubo are clearly identified from the coupled signatures of decreased ozone and increased temperature, opposite to the positive ozone-temperature correlations observed at other times. The ratios of ozone to temperature anomalies derived here show quantitative signatures indicating that either radiative (trend, solar, and QBO) or dynamical (ENSO and residuals) processes are responsible for the strong ozone-temperature correlations.

1. Introduction

Much of the observed variability of stratospheric ozone and temperature on monthly to interannual timescales is attributable to trendlike changes, or to forced variations with specified timescales. Trendlike decreases in total ozone have been reported by *Stolarski et al.* [1991, 1992], while negative temperature trends in the lower stratosphere have been shown in the results of *Angel* [1988], *Karoly* [1989], and *Miller et al.* [1992]. Signals of forced variations in ozone data have been reported for the solar cycle [*Angel*, 1989; *Hood and McCormack*, 1992], quasi-biennial oscillation (QBO) [*Hasebe*, 1980; *Bowman*, 1989], and El Niño-Southern Oscillation (ENSO) [*Shiotani*, 1992; *Zerefos et al.*, 1992]. Similar signals in stratospheric temperature and circulation data have also been observed [e.g., *van Loon and Labitzke*, 1990; *Holton and Tan*, 1980; *Karoly et al.*, 1992; also *Dunkerton and Baldwin*, 1992]. For the QBO signal in particular, it is well known that total ozone and lower stratospheric temperature anomalies are strongly correlated over the equator [*Lait et al.*, 1989; *Chandra and Stolarski*, 1991]. Such positive ozone-temperature correlations have also been noted in extratropics on interannual timescales [*Labitzke and van Loon*, 1992] as well as for variations of individual monthly means [*Newman and Randel*, 1988].

The objective of this study is to make a systematic analysis of long time series of total ozone and lower stratospheric temperature data to (1) determine the space-time structure of ozone-temperature coherence for trends and signals attributable to the above forcing mechanisms and (2) analyze the coherence between the residuals of the respective time series (due to the month-to-month variability inherent to the atmosphere). We utilize ozone and temperature data which are of high quality, with documented calibration limits over the 14-year record investigated here, namely, total ozone mapping spectrometer (TOMS) version 6 ozone and microwave sounding unit (MSU) channel 4 temperature data. Our focus here is on timescales of monthly means and longer (thus excluding the effects of baroclinic waves [*Schoeberl and Krueger*, 1983; *Mote et al.*, 1991] and reducing the effects of 30- to 60-day oscillations [*Gao and Stanford*, 1990]). We use a linear regression model to estimate the trend, solar cycle, QBO, and ENSO variations in ozone and temperature individually (following the analysis of *Stolarski et al.* [1991]), and we examine the importance of the terms with respect to each other and also their evolution with respect to latitude and season. Furthermore, residuals of the ozone and temperature data are analyzed (defined as the deseasonalized total minus linearly related variations calculated by the regressions) to determine the coherence between month-to-month "natural variability" of these fields.

Paper number 93JD03454.
0148-0227/94/93JD-03454 $05.00

There are two mechanisms whereby total ozone and lower stratospheric temperatures are positively correlated. One is due to dynamically induced variations: the background gradients of ozone and (potential) temperature are such that both vertical and meridional parcel motions result in positively correlated ozone and lower stratospheric temperature anomalies [*Newman and Randel*, 1988; *Tung and Yang*, 1988; *Wirth*, 1993]. Secondly, radiative effects lead to positively correlated anomalies: reduced ozone density in the lower stratosphere (and hence column ozone) results in less radiative heating and hence decreased equilibrium temperatures [e.g., *Shine*, 1986; *Kiehl et al.*, 1988; *Miller et al.*, 1992]. The radiative effects should become important for timescales longer than the radiative relaxation time in the lower stratosphere, of the order of 50-100 days. Thus for the long timescale variations considered here, both mechanisms are potentially important. In section 5 we quantify these different mechanisms according to the expected ratios of ozone change to temperature change (derived from the above studies). These theoretical results are in reasonable agreement with the ratios calculated from the data here and allow us to demonstrate that either radiative (trend, solar, and QBO signals) or dynamical (ENSO and residuals) processes are responsible for the high ozone-temperature correlations observed here.

2. Data and Analyses

The total ozone data analyzed here are from the TOMS instrument on the Nimbus 7 spacecraft, covering the 14 years 1979-1992. We use the most recently reprocessed TOMS data (version 6), which have been adjusted to remove the long-term drifts attributable to the TOMS instrument. Monthly average ozone fields were sampled on a regular 5° latitude by 10° longitude grid. The mean seasonal cycle was calculated by averaging each month over the 10 years of data 1982-1991, and this seasonal cycle was subtracted from each monthly average to produce 168 (14 years × 12 months) monthly mean anomalies. These time series were then smoothed with a 1-2-1 filter in time to remove the highest-frequency variations. TOMS data are not available in polar night regions, and these are hence excluded in our analyses.

The temperature data used here are from channel 4 of the MSU instrument, which has been incorporated on a series of NOAA operational satellites. Channel 4 measures the thermal radiation emitted from an atmospheric layer centered between approximately 50-150 mbar (13-22 km), with a maximum response near 90 mbar (17 km), as shown by the instrumental weighting function in Figure 1. Over extratropical latitudes poleward of approximately ± 30°, these weighted temperatures lie almost entirely within the lower stratosphere. In the tropics, however, the tropopause occurs near the weighting function maximum, so that the signal is weighted between the upper troposphere and lower stratosphere. For reference, Figure 1 also shows the temperature trends over Northern Hemisphere (NH) midlatitudes deduced by *Miller et al.* [1992]; note that the cooling in the lower stratosphere occurs over the same altitude region as that sampled by MSU channel 4.

The MSU instrument scans horizontally across the satellite orbital track, and the effective weighting function moves progressively upward with scan angle because the atmospheric transmission path becomes more oblique. This scan angle effect has been removed in the data used here by linear regression of each scan position against the nadir view [*Spencer and Christy*, 1993]. Monthly mean data were obtained for the period 1979-1992, and these data were sampled on the same 5° × 10° horizontal grid used for the ozone data. Likewise, the mean seasonal temperature cycle

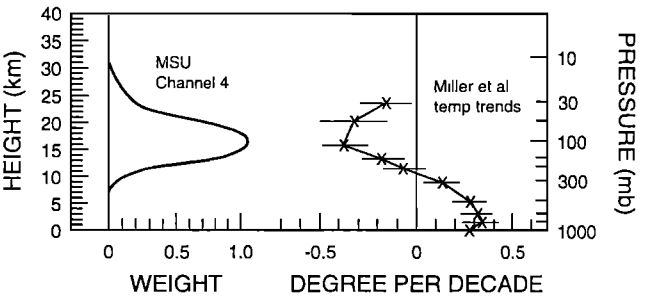

Figure 1. (Left) Weighting function for microwave sounding unit (MSU) channel 4 temperature measurements. (Right) Temperature trends derived from global radiosonde data, taken from *Miller et al.* [1992].

was calculated over 1982-1991 and subtracted from each month's data to produce 168 monthly temperature anomalies. These were also smoothed with a 1-2-1 filter in time. Although these temperature data have been derived from seven separate MSU instruments during 1979-1992, *Spencer and Christy* [1993] have shown that the sensors are very stable in their calibration, and very small (≤ 0.01 K) intersatellite changes are observed.

Linear regression analysis is used to isolate and remove specific signals from the ozone and temperature anomaly time series. The regression model used for ozone is

$$O_3(t) = \alpha\ \text{trend} + \beta\ \text{solar} + \gamma\ \text{QBO} + \varepsilon\ \text{ENSO} + \text{residual}, \quad (1)$$

and likewise for temperature. The choice of using these parameter fits is based on a similar analysis of TOMS data by *Stolarski et al.* [1991], together with the ENSO signal found in TOMS data by *Shiotani* [1992]. To fit seasonal variability, the coefficients α, β, γ, and ε in (1) all have the form $\alpha = (A_1 + A_2 \cos \omega t + A_3 \sin \omega t + A_4 \cos 2\omega t + A_5 \sin 2\omega t + A_6 \cos 3\omega t + A_7 \sin 3\omega t)$, with $\omega = 2\pi/12$ months. Each term in (1) thus has seven parameters to be determined, and there are a total of 28 parameters fit to the time series by the least squares analysis. Note that the trend term in (1) is implicitly nonlinear (with terms like $t \sin \omega t$), and the results of such fits can be unreliable. To check the representation used here, the data were fit with (1) for each individual month (all the January data, for example); the resulting seasonality in the fits was similar to that shown here but with more month-to-month variability. Further discussion on the details of seasonally varying trend detection can be found in Appendix A of World Meteorological Organization (*WMO*) [1988]. The residual term in (1) is characterized by a first-order autoregressive process, following the calculations of *Stolarski et al.* [1991]. Error estimates for the statistical fits are estimated according to [*Neter et al.*, 1985, chapter 7]:

$$\sigma^2(\alpha) = \left[\sigma^2(A_1) + \sigma^2(A_2)\cos^2 \omega t + \sigma^2(A_3)\sin^2 \omega t + \ldots + 2\cdot\left(\sigma(A_1,A_2)\cos \omega t + \sigma(A_1,A_3)\sin \omega t + \ldots\right)\right] \quad (2)$$

Here the $\sigma^2(A_1)$ and $\sigma^2(A_1,A_2)$, etc., are variance-covariance estimates of the regression coefficients, obtained from the least squares analysis. Shaded regions in all of the latitude-time diagrams below indicate where the statistical fits are not significantly different from zero at the 2σ level. Error estimates for the trends include instrumental trend errors of 0.13% per year for ozone [*Stolarski et al.*, 1991] and 0.01 K/yr for MSU temperature

(estimated from the 0.01 intersatellite variations derived by *Spencer and Christy* [1993]). The reference solar cycle time series is the smoothed 10.7-cm solar radio flux, that for the QBO is taken from monthly mean 30-mbar tropical winds, and the ENSO time series is a normalized Southern Oscillation index (SOI); these reference time series are shown in Figure 2. Note that none of these reference time series is temporally lagged here, as we did not find a significant improvement in the associated fits by adding such further parameters. The reference time series are each normalized to have zero time mean prior to the regression analysis.

Global ozone, as measured by TOMS, was particularly low over large regions of the globe during much of 1992 [*Gleason et al.*, 1993], possibly related to the eruption of Mount Pinatubo in June 1991. Because we do not want the anomalous 1992 data to affect our statistical regression fits, we perform the regression (1) using only data from 1979-1991. To calculate residuals, the model is extended into 1992 using the derived regression parameters, together with known solar, QBO, and ENSO indices.

As examples, time series of zonal mean ozone and temperature at 60°S over the entire record 1979-1992 are shown in Figures 3 and 4. The top curves show the actual monthly mean values, with strong seasonal cycles in both quantities. Ozone and temperature variations with the seasonal cycles removed are shown as solid curves in the bottom halves of Figures 3 and 4, together with time series derived from the trend, solar, QBO, and ENSO variations determined from the linear model in (1) (shown as dashed curves). Several features may be noted from Figures 3 and 4 regarding the anomalies and their fits by (1):

(1) The ozone and temperature anomalies are positively correlated with each other in time; note the alternating positive and negative variations in each series over 1985-1989.

(2) The linear model fit of the ozone anomalies explains much more of the overall variance than the corresponding fit of the temperature anomalies. This is true over most of the globe: the linear model accounts for approximately 60-80% of the ozone variance but only 20-60% of the temperature variance (depending on latitude and season).

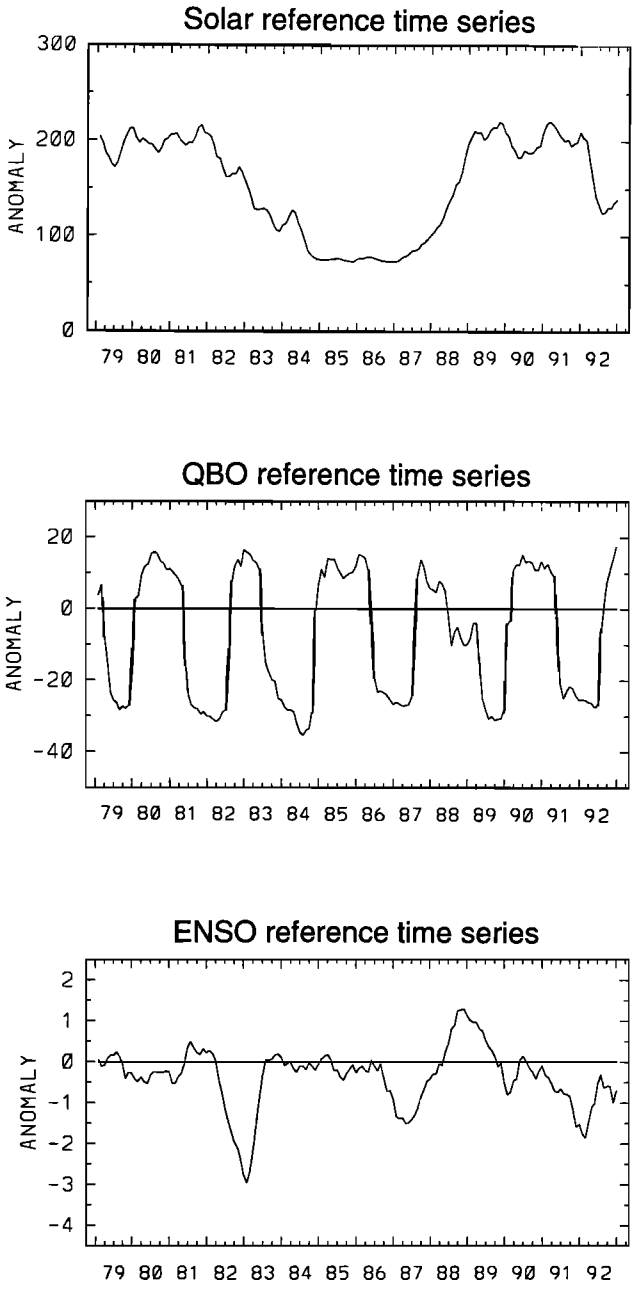

Figure 2. Reference time series used for the regression analyses. (Top) F10.7-cm solar flux, (middle) 30-mbar zonal winds over the equator, and (bottom) normalized Tahiti minus Darwin sea level pressure (southern oscillation index (SOI)).

3. Fits to Regular Signals

3.1. Trend and Solar Signals

This section discusses the space-time structure of the calculated ozone and temperature fits to the individual terms in (1). The trend and solar cycle signals are discussed together because the results show a space-time relationship between the two signals; the predominant global variations project mathematically as a combination of linear trend and solar signal over 1979-1991. We note that projections onto the solar cycle for the short time series analyzed here are suspect as to direct association with solar forcing; these projections mainly highlight regions of decadal-scale

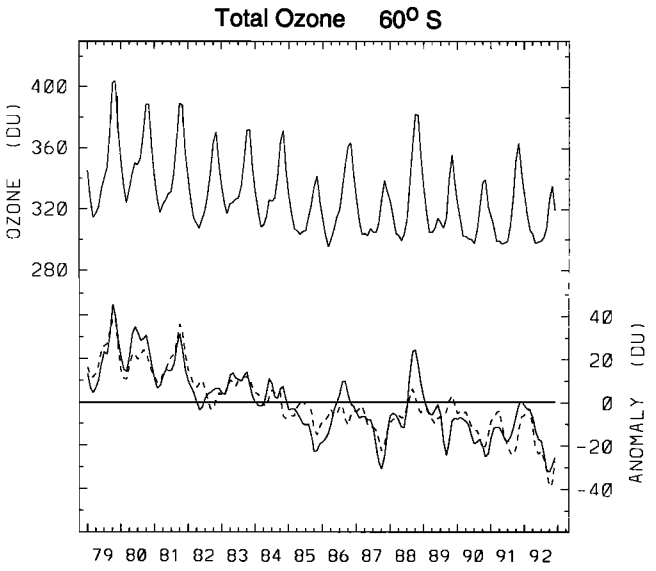

Figure 3. Top curve shows zonal mean total ozone mapping spectrometer (TOMS) total ozone at 60°S. Solid curve at the bottom shows the deseasonalized anomalies, and the dashed curve is the regression fit derived from (1).

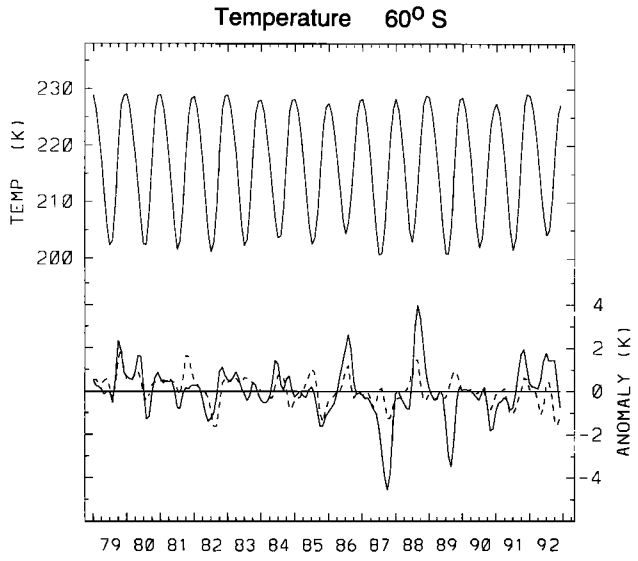

Figure 4. Top curve shows zonal mean MSU temperatures at 60°S. Solid curve at bottom shows the deseasonalized anomalies, while the dashed curve is the regression fit from (1).

variation which happen to be roughly in phase with the solar signal but could also occur due to a number of other physical processes (such as atmosphere-ocean coupling or phase beating of the QBO and annual cycle). In spite of this caveat the solar cycle patterns derived here are in basic agreement with prior studies utilizing data over approximately three solar cycles [*van Loon and Labitzke*, 1990; *Dunkerton and Baldwin*, 1992] (see discussion below).

Figure 5 shows the calculated ozone and temperature trends versus latitude and month. The ozone trends shown here are nearly identical to the results shown by *Stolarski et al.* [1991], except the contours here are Dobson units (DU)/year, rather than percent/year. Significant negative ozone trends are found in the NH extratropics throughout winter-spring and in SH extratropics throughout the entire year (maximizing over the Antarctic during September-October). The calculated temperature trends in Figure 5 show significant negative values over NH midlatitudes during January-June and large (but not statistically significant) cooling over polar regions during March-April. SH trends show significant negative values over the Antarctic during October-November and during the summer (December-April) over 30°-50°S. The patterns of ozone and temperature trends are well correlated during NH winter-spring. During SH winter-spring the maximum temperature trends occur approximately 1-2 months later than the maximum ozone trends (November versus September-October); note that this delay is in reasonable agreement with the simulation of *Kiehl et al.* [1988] and is related to the return of the Sun to high latitudes and the radiative relaxation time (of the order of 2 months) in the lower stratosphere. Temperature trends show near-zero values in SH middle-high latitudes during late winter (July-September), in contrast to the strong negative ozone trends observed during this time. Note that this period is outside of polar night (as indicated in Figure 5 (bottom), so that a radiative response to the observed ozone depletion is expected.

Figure 6 shows time series of ozone and temperature anomalies for selected months and latitudes, chosen based on Figure 5. The top and bottom panels are for the NH winter midlatitude and SH spring polar regions, respectively, where significant negative trends are found in both ozone and temperature. These figures show correlated behavior between these time series for individual yearly anomalies, in addition to the downward trends in both variables. The middle panel in Figure 6 shows the anomalies at 60°S during July-August, where the ozone shows a downward trend but the temperatures do not. Note that aside from the different trends at this location the yearly anomalies still show some correlation between ozone and temperature.

Figure 7 shows the solar signals in ozone and temperature derived from the regression analyses. Ozone shows a statistically significant positive response to the solar signal mainly over the subtropics of both hemispheres (approximately 10°-40°N and S), with an additional positive maximum in SH high latitudes during October-December. The largest magnitude responses (of size 10 DU between solar maximum and minimum) are found in NH winter-spring over 20°-40°N and in SH spring over 60°S-pole, in roughly the same location and time as the maximum (negative) ozone trends seen in Figure 5.

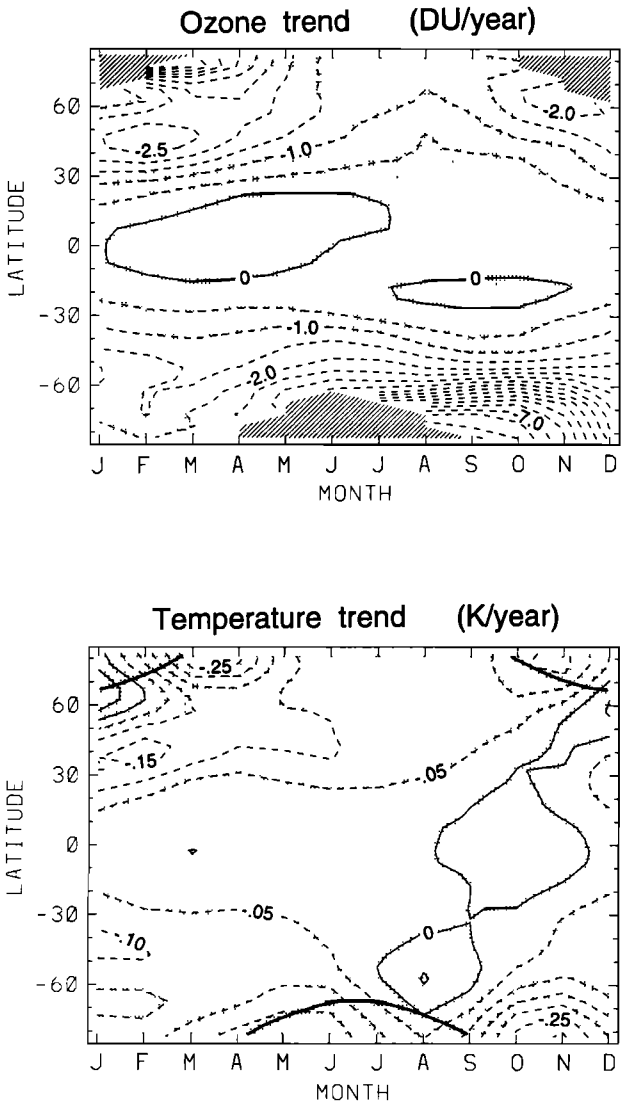

Figure 5. Latitude-time sections of the zonal mean ozone and temperature trends, calculated from data over 1979-1991, with units of DU/year and K/year, respectively. Stippling denotes regions where the statistical fits are not different from zero at the 2σ level. Hatched regions in the top panel denote polar night, where no ozone data are available. For reference, polar night regions are also denoted by thick lines in the bottom panel.

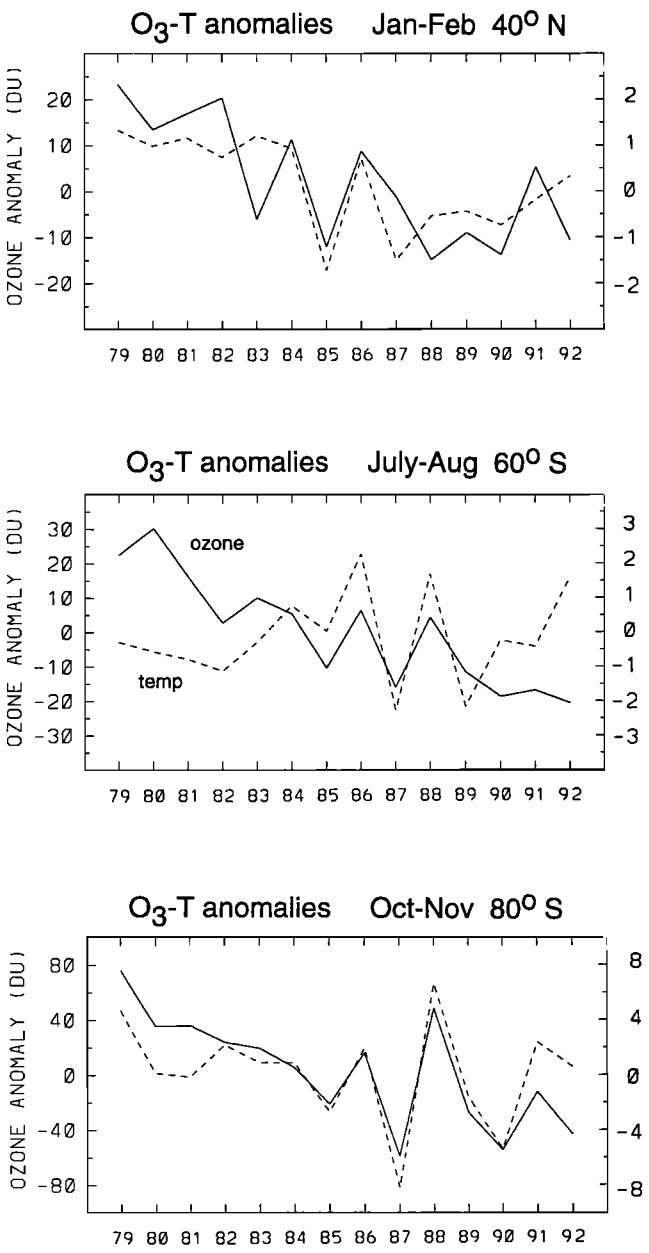

Figure 6. Two-month averages of deseasonalized ozone and temperature anomalies over 1979-1992, at several locations chosen based on Figure 5. (Top) January-February at 40°N, (middle) July-August at 60°S, and (bottom) October-November at 80°S.

The similarly positioned maxima (of opposite sign) seen in the derived ozone trend and solar signals suggest that there may be some coupling between these terms in the analyses here. An independent analysis not tied to either linear trend or solar signal was made by using an empirical orthogonal function (EOF) analysis of the latitude-month variation of the interannual ozone anomalies. In this analysis the ozone anomalies were area (cos (latitude)) weighted, and only data over 1979-1991 were included. Figure 8 shows the structure of the resulting first EOF, which accounts for 78% of the overall interannual variance, together with the time variation over 1979-1992 of the projection of EOF 1 onto the global ozone anomalies. The latitude-month patterns in Figure 8 show maxima over middle latitudes of the NH and middle-to-polar latitudes of the SH during the respective winter and spring seasons, qualitatively similar to both the trend and the solar signals shown in Figures 5-7. The time variation of EOF 1 (bottom of Figure 8) shows a strong decrease over 1979-1985, followed by near-constant values over 1986-1991, and low values in 1990 and 1992. Note the overall agreement with the actual anomaly time series shown in Figure 6. This time variation projects mathematically as a negative linear trend plus a positive fraction of the solar signal; this results in the similar spatial patterns seen in Figures 5-7. There are two possible explanations for this overall behavior: (1) the spatial patterns of the trend and solar influence are in reality similar and of opposite sign or (2) projection onto the solar signal is an artifact, introduced by the flattening of the negative trends after 1985. It is difficult to distinguish between these possibilities based on the short date record here. In either case, the patterns seen in Figure 8 are intriguing in that the variations are truly global in nature, with ozone changes that are coherent between the hemispheres (maximizing during the respective winter-spring seasons).

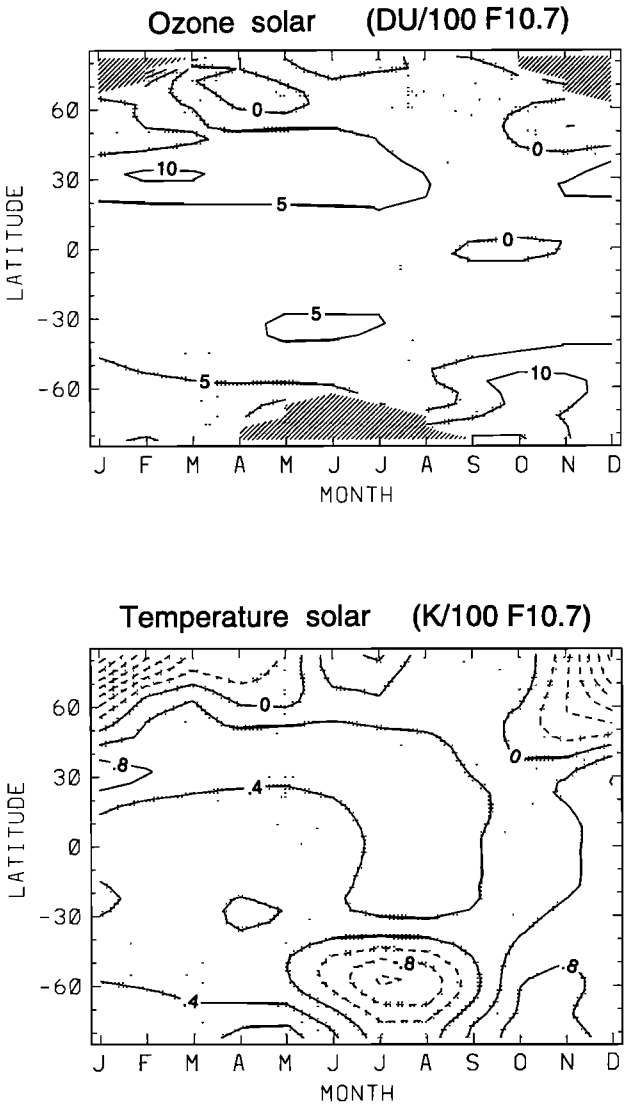

Figure 7. Latitude-time sections of the solar cycle regression fits over 1979-1991 for zonal mean ozone and temperature, with units of DU or K per 100 units of F10.7-cm solar flux (see Figure 2).

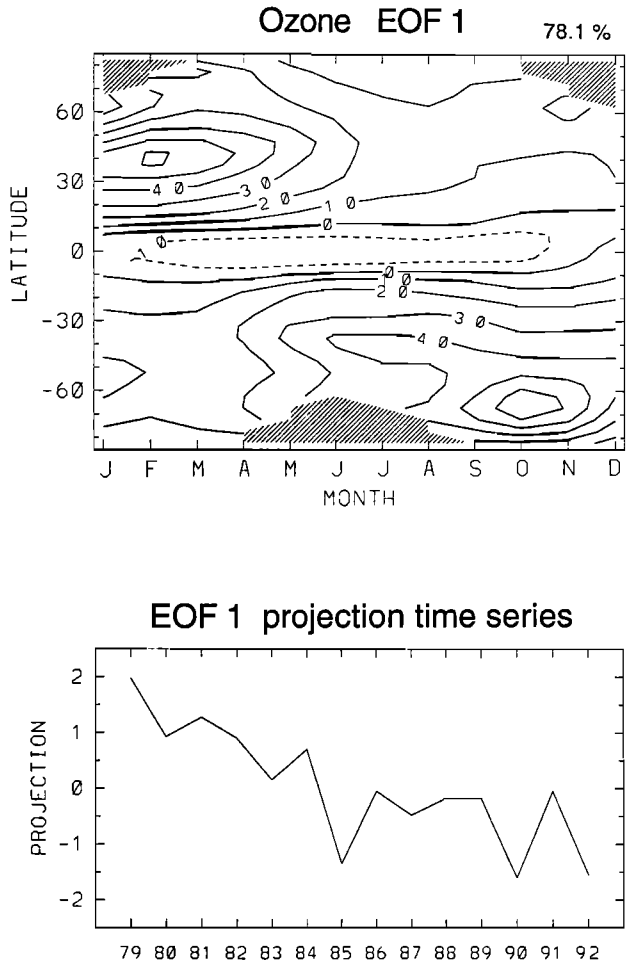

Figure 8. (Top) Structure of the first empirical orthogonal function (EOF) of latitude-month variability of zonal mean total ozone over 1979-1991. (Bottom) Time projection over 1979-1992 of EOF 1. Units are arbitary.

The solar cycle temperature signal in Figure 7 shows a significant positive pattern over approximately 20°-50°N for most of the year (excluding fall), similar in structure to the observed ozone pattern in Figure 7. This temperature signal is in agreement with solar signal correlation patterns for 30-mbar geopotential height presented by *van Loon and Labitzke* [1990]; this is reasonable because the 30-mbar height is hydrostatically related to the lower stratospheric layer mean temperature measured by MSU channel 4 (see Figure 1). This maximum in NH midlatitudes is what they term the "basic pattern"; note their analyses cover a much longer time series of data (1958-1987). The patterns in Figure 7 also show additional structure during December-January in the NH and July-August in the SH: negative projections in high latitudes, coupled with positive signals over the tropics and subtropics (approximately 40°N-S). The symmetry of these patterns between the winter hemispheres is suggestive of a true signal. The temperature anomalies which contribute to this negative solar cycle projection during July-August at 60°S are shown in the middle panel of Figure 6; note this is the location where the ozone shows a strong downward trend but the temperatures do not. Although such fits to the solar cycle are questionable due to the short record here, *Dunkerton and Baldwin* [1992] show a similar negative temperature correlation over NH polar latitudes in December-January, based on data covering 1964-1990 (their Figure 3). Note that there are strong meridional temperature gradients in winter middle latitudes inferred in Figure 7, which will be in balance with increased vertical wind shears. *Kodera and Yamazaki* [1990] and *Kodera* [1991] have shown observations suggestive of increased stratospheric westerlies in early NH winter which are in phase with the solar cycle, consistent with the temperature gradients seen here.

Figure 9 shows latitude-longitude plots of the trends in ozone and temperature during January-February. In high NH latitudes the temperature trends show a pronounced zonal wave 1 pattern, with large negative trends over eastern Asia and positive trends over the far North Atlantic. A similar (in phase) zonal structure is seen in the high northern latitude ozone trends (which can only be analyzed to 68°N during this period; *Niu et al.* [1992] have shown similar ozone trend results). This zonal wave structure is strongly suggestive of a dynamical origin for this variability, i.e., a shift in the climatological stationary waves with as decadal timescale [e.g.,

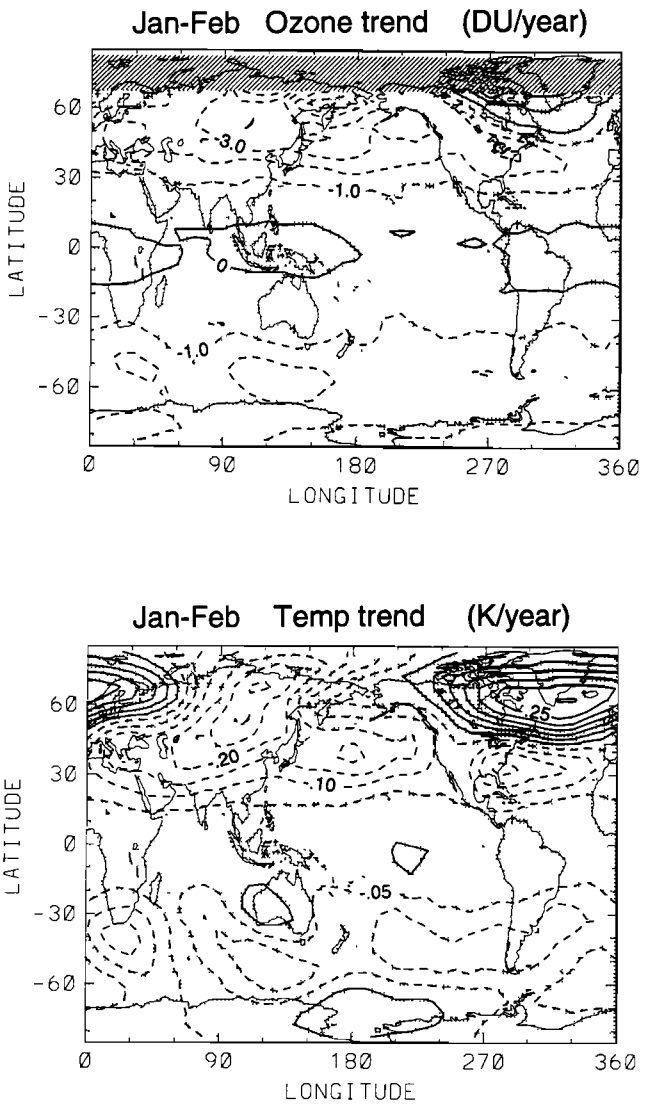

Figure 9. Latitude-longitude diagrams of ozone and temperature trends during January-February for data over 1979-1991. No ozone data are available in the hatched region poleward of 68°N in the top panel.

Trenberth, 1990]. The strong negative trends over Siberia in Figure 9 occur in a region where the climatological stationary wave structure is a maximum (in both ozone and temperature), so that these trends represent a weakening of the climatological wavy structure. There is less zonal structure to the trends in the midlatitude band 30°-50°N, but the longitudinally localized maxima that are evident are mirrored in both ozone and temperature (for example, the negative maximum over the eastern United States).

3.2. QBO Signal

Interannual variability of total ozone in the tropics is observed to be dominated by the QBO [*Hasebe*, 1980; *Shiotani*, 1992]. This is clearly shown in Figure 10, where the monthly mean data are shown together with the deseasonalized anomalies; the latter clearly track the 30-mbar zonal winds (Figure 2). Figure 10 furthermore shows that the QBO is the dominant signal for interannual variations of lower stratospheric temperature (the QBO temperature anomalies of the order of 1 K seen in Figure 10 are representative of the 50- to 150-mbar level; QBO anomalies at somewhat higher levels (30-50 mbar) are of the order of 2-4 K [*Dunkerton and Delisi*, 1985]). Overall, the ozone and temperature QBO signals are in phase, although there appears to be a phase lag of the order of 3-6 months between the ozone and the temperatures during the negative-to-positive anomaly transitions of 1979-1980, 1984-1985, and 1989-1990 (westerly wind accelerations in Figure 2); the signals are more in phase for the slower easterly accelerations (except during 1982-1983 and 1991-1992, when ENSO and volcanic effects are important; see below).

QBO-related variations in total ozone over the globe have been reported in a long series of studies, most recently using TOMS data by *Bowman* [1989], *Lait et al.* [1989], and *Shiotani* [1992]. Figure 11 shows latitude-month diagrams of the ozone and temperature QBO projections determined here by the regression analysis. Similar patterns of QBO ozone variability have recently been shown by *Chandra and Stolarski* [1991]. The similarity in space-time structures of the ozone and temperature QBO projections in Figure 11 is remarkable. Positive values are found over the

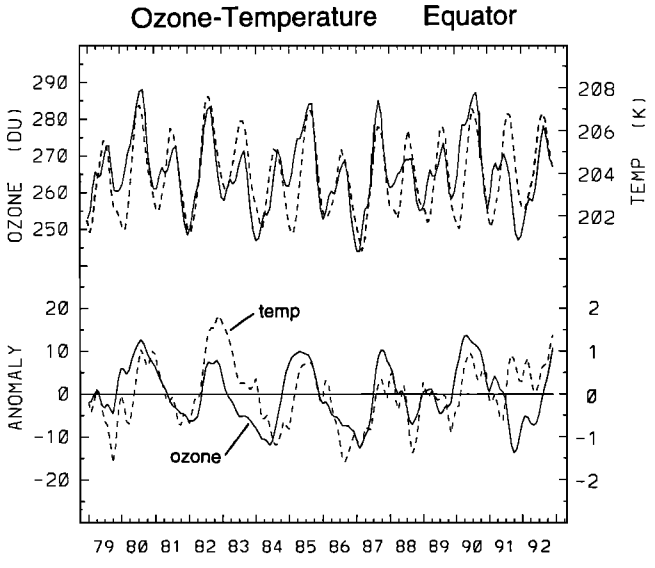

Figure 10. Top curves show total ozone (solid) and MSU temperature (dashed) time series over the equator. Bottom curves are the deseasonalized versions of these data, clearly revealing the quasi-biennial oscillation (QBO) signal in both quantities.

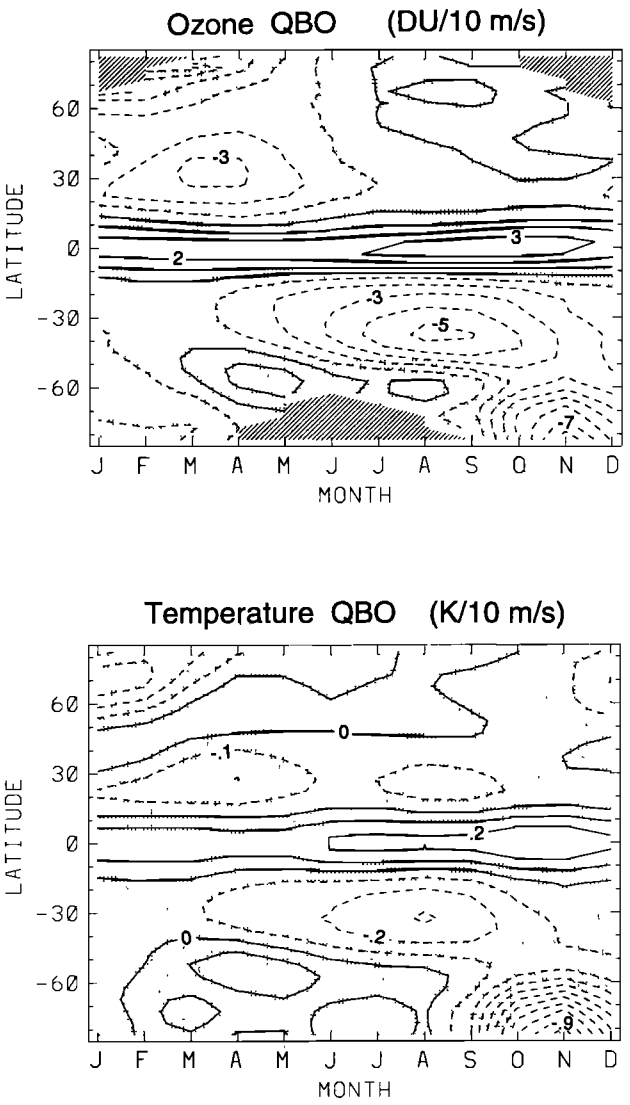

Figure 11. Latitude-time sections of the QBO-associated regression fits of zonal mean ozone and temperature, based on data over 1979-1991. Units are DU or K per 10 m/s of QBO winds (see Figure 2).

equator, covering approximately 10°N-S, with a slight maximum during the second half of the year. Out of phase (negative) maxima are observed in the subtropics of both hemispheres (20°-50°) but only during the winter-spring seasons in each hemisphere. The subtropical anomalies are approximately 1.5 times larger in the SH than in the NH. These subtropical QBO anomalies in total ozone and their seasonal synchronization have been noted before by *Bowman* [1989] and *Hamilton* [1989]. The similar subtropical variations in lower stratospheric temperature seen in Figure 11 have apparently not been discussed before. *Gray and Dunkerton* [1990] have obtained this seasonally synchronized result for total ozone in a two-dimensional model, incorporating an idealized QBO together with an annual cycle, and likewise *Gray and Ruth* [1993] for a similar model incorporating the observed QBO winds. These studies explain the seasonal synchronization in the subtropics as due to interaction of the QBO and annual cycles and, furthermore, show that the subtropical maxima are asymmetric in magnitude between hemispheres (as observed in Figure 11), a result that is

continually modified in time due to the phase interactions of the QBO and annual cycles.

The QBO patterns in Figure 11 also show strong negative values in SH polar regions over October-December and a hint of similar structure over NH high latitudes in winter (barely reaching significant levels). These temperature signals represent modulations in the strength of the winter polar vortexes, which are out of phase with the equatorial QBO. These associations have been studied by *Angel and Korshover* [1964], *Holton and Tan* [1980], and most recently by *Dunkerton and Baldwin* [1992], who find similar QBO temperature patterns in high northern latitudes during winter, based on a much longer data set (1964-1991) than that used here. *Garcia and Solomon* [1987] first noted the association between the depth of the Antarctic ozone hole and the QBO, and *Lait et al.* [1989] have analyzed this relationship in some detail. At present the cause of this behavior is not well understood, although QBO modulation of stratospheric planetary waves produces similar effects in numerical models [*O'Sullivan and Young*, 1992].

3.3. ENSO Signal

Shiotani [1992] has shown clear evidence of an ENSO signal in total ozone over the tropics, in the form of an east-west seesaw pattern between the eastern and the western Pacific Ocean basins; the signal is less apparent in zonal mean fields. We thus examine the ENSO signal here in terms of latitude-longitude structure over the globe, rather than in zonal mean data. We furthermore separate the observed patterns between NH and SH winter-spring seasons (January-May and July-November), because we find strong seasonality in the calculated patterns. Figures 12-13 show the calculated ENSO patterns in ozone and temperature separated accordingly.

The NH winter patterns in temperature (bottom, Figure 12) are most remarkable, showing three centers of negative anomalies in the subtropics-midlatitudes of each hemisphere, paired symmetrically about the equator with patterns in the other hemisphere. The negative patterns in the eastern Pacific are observed at higher latitudes (near 45°N-S) and sandwich a pair of positive anomalies near 15°N-S. This lower stratospheric temperature structure in the eastern Pacific mirrors (with opposite sign) that observed throughout the troposphere during ENSO events [e.g., *Horel and Wallace*, 1981; *Meehl and Albrect*, 1991; *Yulaeva and Wallace*, 1994]. Dynamically, this tropospheric structure in the eastern Pacific is evidenced as a pair of anticyclonic centers in the upper troposphere centered near 15°N-S [*Blackmon et al.*, 1983], which occur as the atmospheric response to enhanced tropical heating in the eastern Pacific during ENSO. The temperature patterns during SH winter (Figure 13) have similar latitude-longitude structure, but they are superimposed over a large negative zonal mean response in the tropics (over approximately 30°N-S). This zonal mean cooling of the tropical lower stratosphere during ENSO events has been shown previously [*Pan and Oort*, 1983; *Meehl and Albrect*, 1991; *Karoly et al.*, 1994], and is coupled to a zonal mean warming throughout the tropical troposphere. Additionally, Figures 12-13 show large amplitude stationary wave 1 temperature anomalies in high latitudes of both winter hemispheres.

The ozone patterns in Figures 12-13 are similar overall to the temperature structures but with less symmetry with respect to the equator (showing large-amplitude responses mainly in the respective winter hemispheres). Furthermore, there is not an added zonal mean response in the tropics during SH winter, as that seen in the temperatures. The seesaw pattern between the eastern and the western Pacific basins noted by *Shiotani* [1992] is evident upon close inspection, particularly in the SH winter. However, the most conspicuous ozone anomalies are the coupled north-south dipole patterns in the Pacific region, with the largest amplitudes in the respective winter hemispheres. As with the temperature patterns, ozone shows a large stationary wave 1 in high winter latitudes. Note that the negative patterns in Figures 12-13 are particularly strong year-round in the South Pacific (stronger in SH winter). Figure 14 shows time series of ozone and temperature anomalies in an area near 45°S, 210°E; here we have subtracted the variations due to trend, solar, and QBO signals. Figure 14 also includes the ENSO reference time series (from Figure 2), and strong anticorrelation between these time series is evident (note the enhanced responses during SH winter seasons in Figure 14).

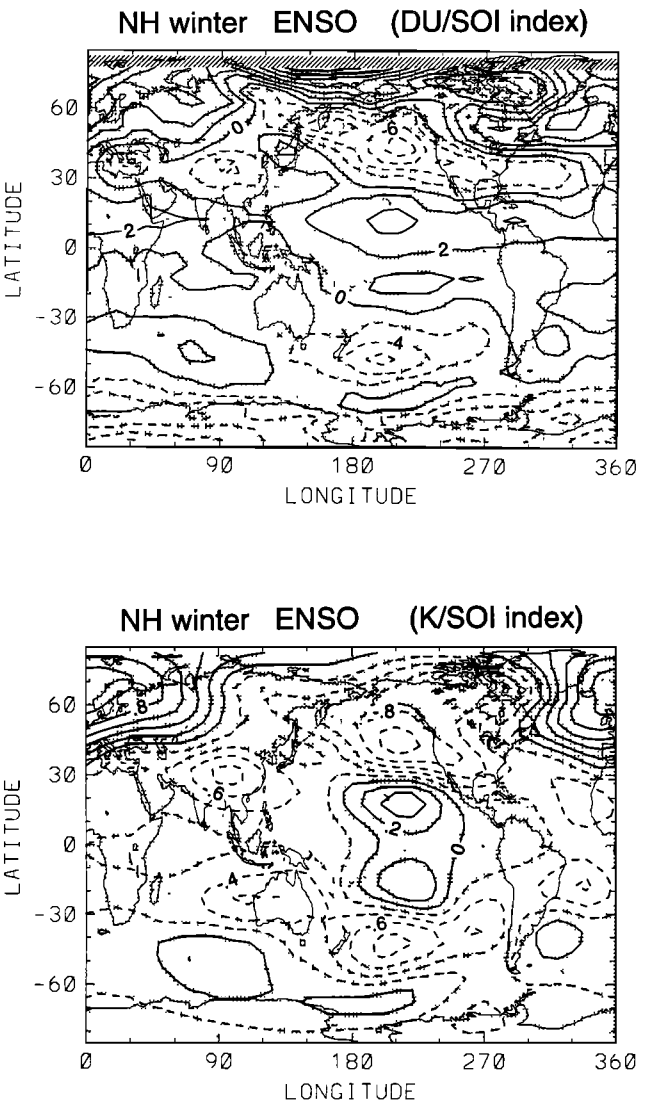

Figure 12. Latitude-longitude plots of the El Niño-Southern Oscillation (ENSO) related ozone and temperature variability during Northern Hemisphere (NH) winter-spring (January-May). Units are DU or K per normalized SOI index (see Figure 2).

4. Residuals

This section considers the degree of correlation between monthly mean ozone and temperature residuals over the globe.

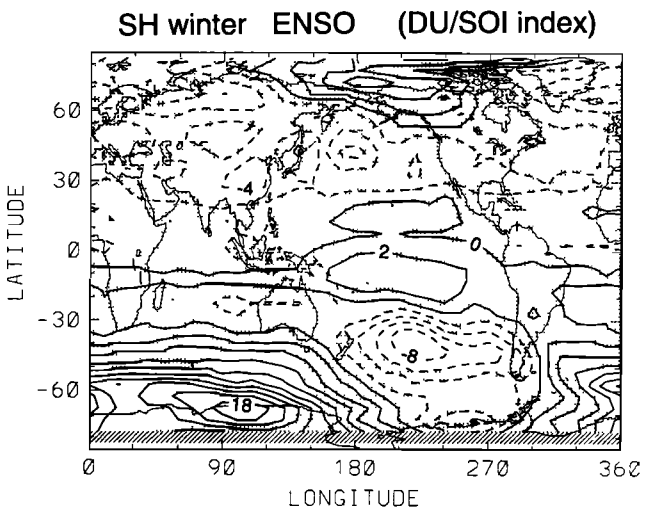

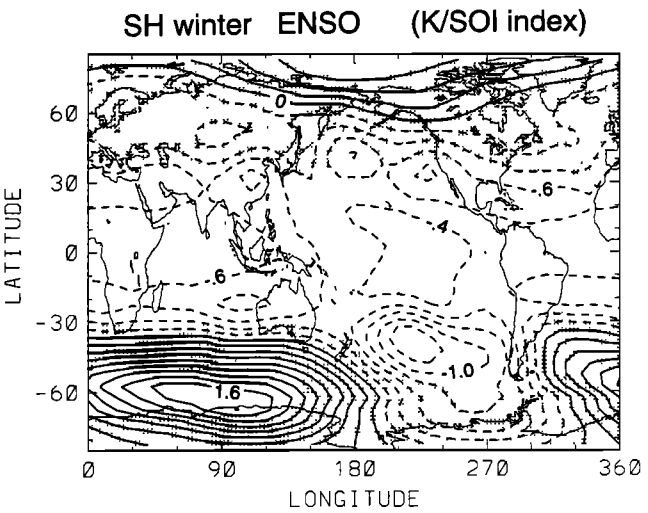

Figure 13. Ozone and temperature ENSO projections during Southern Hemisphere (SH) winter-spring (July-November).

Residuals are defined to be the deseasonalized anomalies analyzed above, minus the calculated trend, solar, QBO, and ENSO signals discussed in section 3 (e.g., the differences between the lower curves in Figures 3-4).

4.1. Zonal Means

Figure 15 shows time series of zonal mean ozone and temperature residuals at latitudes 60°S, 30°S, 0°, 30°N, and 60°N, and Figure 16 shows the calculated correlation coefficient between the zonal mean residuals at each latitude over 80°N-S. Overall, there is strong positive correlation between the ozone and temperature residuals in the extratropics and weak correlation in the tropics. The residual correlations are stronger in the SH (0.6-0.9) than in the NH (0.2-0.5), and the latter show a distinct minimum over 45°-60°N. Inspection of the individual curves in Figure 15 allows identification of specific time periods during which the anomalies are not well correlated. For example, there are two distinct periods at 60°N when the temperature residuals are negative and ozone residuals are positive (NH winters 1979-1980 and 1986-1987, marked with arrows on the top curve of Figure 15).

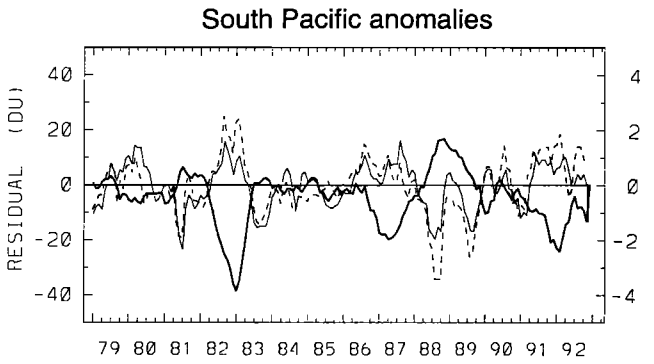

Figure 14. Time series of ozone (solid) and temperature (dashed) anomalies in the South Pacific (near 45°S, 210°E), along with the SOI reference time series (thick solid curve). The trend, solar, and QBO signals have been removed from both anomaly time series.

These events are fairly limited in latitude, contributing to the minimum in correlation over 45°-60°N seen in Figure 16; their cause is unknown.

The relatively weak zonal mean residual correlations in the tropics can be traced primarily to two causes. Part of the poor

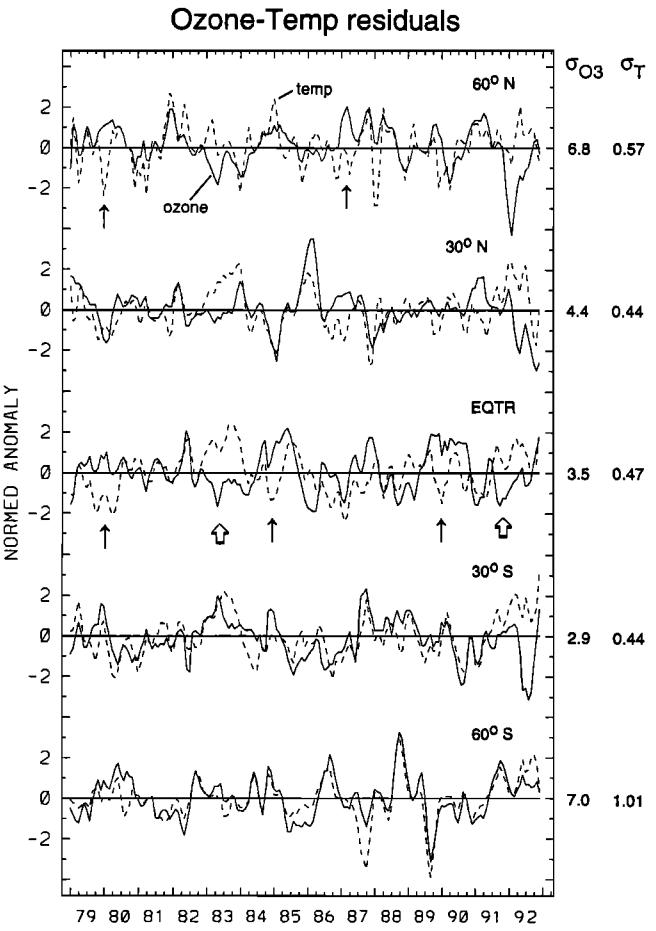

Figure 15. Time series of zonal mean ozone (solid) and temperature (dashed) residuals at the indicated latitudes. The anomalies have been normalized by their respective standard deviations at each location, which are noted on the right side. Arrows denote time periods when the ozone and temperature residuals are particularly uncorrelated, as discussed in text.

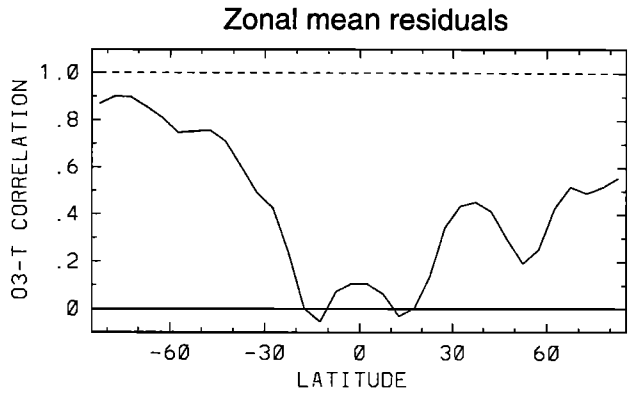

Figure 16. Latitudinal structure of the cross correlation between zonal mean ozone and temperature residuals.

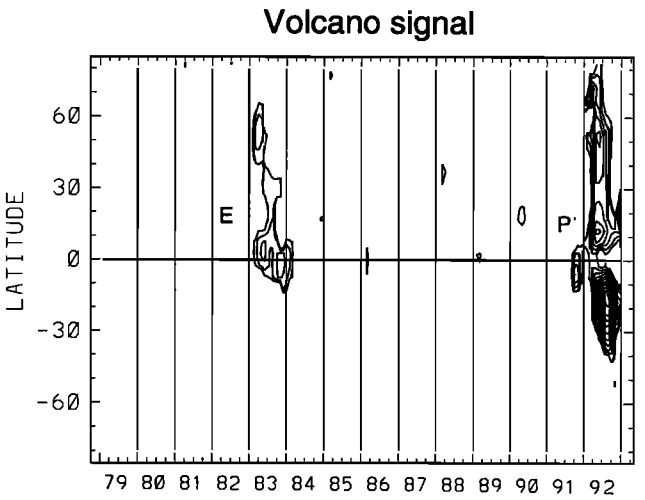

Figure 17. Latitude-time section of the "volcano signal" V (3). Contours are 1.5, 2.0, 2.5, ... E and P denote the eruptions of El Chichon and Pinatubo, respectively.

correlations are due to the ozone-temperature QBO phase differences during the westerly acceleration phases of 79-80, 84-85, and 89-90 (light arrows in the middle of Figure 15), as discussed above in relation to Figure 10. The other important factors at the equator are the temperature increases and ozone decreases associated with the volcanic eruptions of El Chichon and Pinatubo (noted with the outlined arrows in Figure 15). Warming of the lower stratosphere subsequent to these volcanic eruptions has been documented [*Labitzke et al.*, 1983; *Labitzke and McCormick*, 1992] and reduction of ozone levels has also been reported [*Hofmann and Solomon*, 1989; *Schoeberl et al.*, 1993]. *Brasseur and Granier* [1992] have calculated both the temperature and the ozone effects in a numerical model, and *Chandra* [1993] has discussed a volcano signature similar to that identified here.

We quantify the structure of the "volcano signal" (V) in these data according to the normalized temperature-ozone differences:

$$V = \left(\frac{T'}{\sigma_T}\right) - \left(\frac{O_3'}{\sigma_{O_3}}\right) \quad \text{if } T' > 0$$

$$\text{and } O_3' < 0$$

$$V = 0 \qquad \text{otherwise} \qquad (3)$$

where σ_T and σ_{O_3} are the respective time standard deviations at each latitude. Figure 17 shows a latitude-time map of the "volcano signal" (V), showing a distinctive signature following each eruption. The El Chichon signal is observed throughout the tropics and into the NH high latitudes, with a time delay of approximately 1 year. Likewise, the largest Pinatubo signal is seen over large portions of the globe in 1992, nearly a year after the eruption (although a tropical signal is identified in the latter half of 1991 in Figure 17; see also *Chandra* [1993]). It should be noted that tropical warm temperature signals during both 1982-1983 and 1991-1992 were also contributed by the strong ENSO events during these times (e.g., Figures 2 and 13), so that there is necessarily some confusion of the ENSO and volcano signatures in the tropics (i.e., the ENSO temperature signal could be overestimated or the volcano signal underestimated by overlapping of these events).

According to the calculations of *Brasseur and Granier* [1992] the primary cause of the tropical volcano signal is in situ radiative heating due to the volcanic aerosol, and dynamical ozone decrease due to the associated induced upward motion. The causes of the extratropical volcano signals are less well understood. Propagation of the El Chichon aerosols to the NH (but not SH) extratropics was documented by *McCormick and Swissler* [1983], and likewise global dispersion of the Pinatubo aerosol cloud was described by *McCormick and Veiga* [1992]. In situ radiative heating will also occur in the extratropical aerosol layer; the mechanisms for extratropical ozone losses are not yet identified, although chemical losses due to aerosol-induced reactions are a likely candidate [*Hofmann and Solomon*, 1989].

4.2. Zonal Wave Features

Figure 18 shows a map of the correlations between the zonal wave structures in ozone and temperature residuals, i.e., the zonal mean values have been removed prior to calculation of the

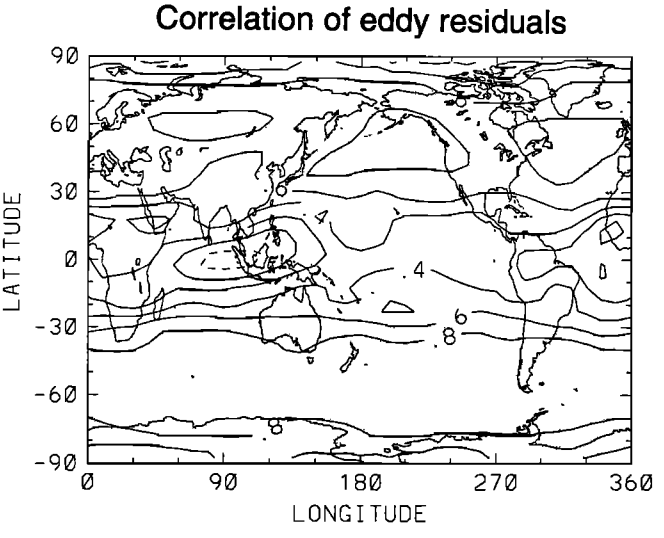

Figure 18. Latitude-longitude plot of the correlation between eddy ozone and temperature residuals (i.e., the zonal means have been removed prior to calculation). The correlations have been spatially smoothed prior to plotting.

correlations. The overall structure shows strong positive correlations (≥ 0.8) in the extratropics of both hemispheres and low correlations in the tropics (over 20°N-S; the tropical correlations are particularly low over Indonesia). The correlations are slightly lower in the NH as compared to the SH, but there is no minimum in correlation over 45°-60°N as found in the zonal mean analyses (Figure 16).

Figure 19 shows the temperature anomalies versus longitude and time at 60°S; the ozone anomalies (not shown) exhibit virtually identical patterns. Large zonal wave number 1 anomalies are observed in the SH winter-spring seasons in Figure 19, with relatively larger amplitudes during the latter half of the record. These wave number 1 anomalies show a preference for phase locking, such that maxima and minima are usually observed near 90° and 270°E. This is the same longitudinal location as the climatological stationary wave 1 in both temperature and ozone (with crests near 110°E; see *Newman and Randel* [1988] and *Wirth* [1993]), so that these anomalies represent primarily an (in phase) intensification or weakening of the climatological stationary wave. Also included in Figure 19 are the zonal mean ozone and temperature anomalies averaged over the SH polar cap (55°-80°S). Comparisons show that the warm, relatively high ozone spring seasons of 1988 and 1991 (and to a lesser degree 1982, 1984, and 1992) are associated with positive wave anomalies near 90°E, i.e., a strengthening of the climatological wave. Conversely, the cold, low ozone years of 1985 and 1989 show negative anomalies near 90°E, i.e., a weakening of the climatological wave. These associations are not surprising, but merely confirm wave-zonal mean flow coupling for these residuals; it is important to note that mechanisms for the stationary wave variations are not well understood. Furthermore, there are examples when the above coupling is not straightforward, most notably 1986 and 1992, when the wave anomalies change sign during the winter, and 1987, when the anomalies are shifted approximately 90° from the climatological positions.

Figure 20 shows longitude-time plots of ozone and temperature anomalies over the equator, where the correlations are low (Figure 18). Maximum temperature anomalies are observed during the NH winter season over the Pacific Ocean, often with the structure of an east-west dipole pattern. Ozone anomalies, on the other hand, do not show evidence of such longitudinal localization. The ozone anomalies in Figure 20 do show features of large scale with persistence for several months period, but we do not see obvious evidence of coherence with other known geophysical variations.

5. Summary and Discussion

The results of this study can be simply categorized in two parts: (1) the coherent ozone-temperature signals derived for the trend, solar signal, QBO, and ENSO variations, resulting from the linear regression analyses, and (2) the associations between the ozone and the temperature monthly mean residuals. These results are summarized in turn here.

The ozone trends are nearly identical to the values recently published by *Stolarski et al.* [1991], showing significant ozone decreases over NH extratropics in winter-spring and over SH extratropics throughout the entire year (maximizing over polar latitudes during August-November, associated with the Antarctic ozone hole). The temperature data analyzed here show significant negative trends in the NH middle-high latitudes during winter-spring, with nearly identical space-time patterns as the NH ozone trends. There are not significant zonal mean trends in either

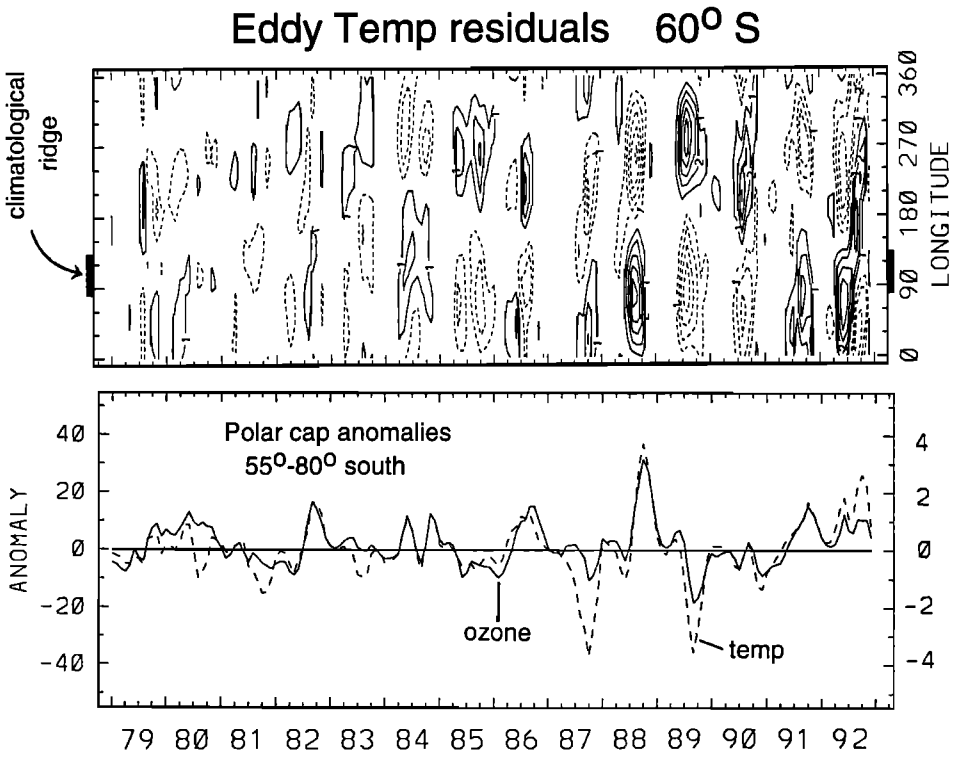

Figure 19. (Top) Longitude-time section of eddy temperature residuals at 60°S. Contour interval is 1 K, with zero contours omitted. (Bottom) Time series of zonal mean ozone (solid) and temperature (dashed) residuals, averaged over the SH polar cap (55°-80°S).

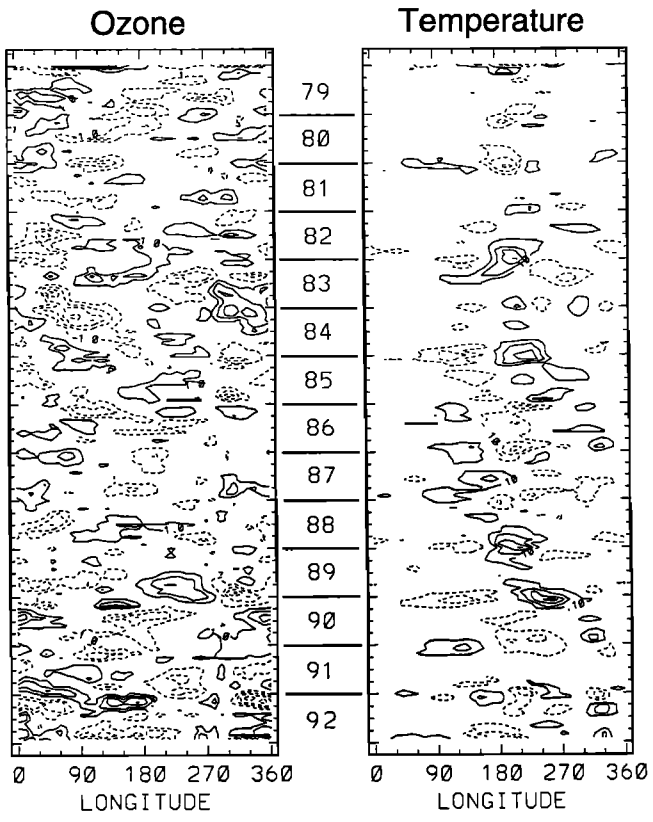

Figure 20. Longitude-time sections of eddy ozone and temperature residuals over the equator. Contours are 1 DU and 1 K, respectively, and zero contours are omitted.

variable over polar regions during midwinter in the NH but rather a strong zonal wave number 1 pattern in both ozone and temperature trends, associated with variability in the climatological stationary wave structure. In contrast to the situation in the NH, significant temperature trends in the SH exhibit patterns that are somewhat different from the ozone trends. Namely, significant negative temperature trends are found only over midlatitudes in summer and over polar latitudes in October-November. Most obvious in these comparisons are the lack of negative temperature trends over middle-high latitudes during midwinter (July-August), although large ozone decreases are observed then (a radiative response to the ozone losses is expected, as this is outside of polar night). Comparisons with the solar signal fit of temperature variations (Figure 7) show that this is precisely the location where large negative solar projections are found, i.e., the lack of negative temperature trends in this region is associated with decadal-scale variations which are out of phase with the solar cycle. A similar negative temperature projection onto solar variations is found in NH polar latitudes in midwinter (see Figure 7), so that the symmetry of these patterns (and their statistical significance) suggests a true signal. Additionally, the same signal has been noted by *Dunkerton and Baldwin* [1992] using a much longer time series of data (1964-1991). Note that these high winter latitudes are the only locations where the ozone and temperature solar projections are fundamentally different.

The other regions of significant solar cycle projections show overall similar patterns in ozone and temperature. Both show positive maxima in NH midlatitudes during winter-spring and in SH middle-high latitudes during spring (in addition, the ozone signal shows significant positive values throughout the subtropical latitude bands 10°-40°N and S over most of the year). The overall similarity in these space-time patterns to those of the calculated trends suggests a possible mixing of these signals over the period analyzed here. An EOF analysis (Figure 8) clearly shows one predominant mode of global ozone variability over 1979-1991, with the time variation of a negative trend plus a positive solar projection. The EOF results are intriguing in that they show true global signatures, with similar magnitude variations during winter-spring in both hemispheres. It is difficult to tell from this analysis alone if the solar influence is real or simply reflects a flattening of the negative trends after 1985. We do note, however, that recent calculations of the solar cycle influence based on general circulation model simulations (K. Kodera, personal communication, 1993) suggest that the positive ozone projections in winter-spring extratropics may be a robust result, due to the effects of planetary wave transport.

The QBO fits of the data here (Figure 11) clearly highlight the (out of phase) winter subtropical ozone maxima documented previously by *Bowman* [1989] and *Hamilton* [1989]; the analyses here show the first evidence of similar signals in lower stratospheric temperature. *Gray and Dunkerton* [1990] have suggested that these subtropical winter signals are not due to planetary wave transport (as might be suspected) but rather to mean vertical motions related to phase locking between the QBO and the annual cycle. As discussed below, the ratio of the ozone to temperature QBO signals suggests that ozone-related radiative processes are important for the temperature response; this finding is in agreement with the recent calculations of *Hasebe* [1994], which suggest that ozone radiative feedbacks are important for the QBO.

The patterns of ENSO-related variability in total ozone shown here complement the recent findings of *Shiotani* [1992], who focused on tropical ENSO influences. The analyses here show that strong ENSO signals are observed well into middle and high latitudes of both winter hemispheres. The extratropical planetary wave patterns in lower stratospheric temperatures documented here are similar to those associated with ENSO-related tropospheric temperatures [e.g., *Meehl and Albrect,* 1991; *Yulaeva and Wallace*, 1993] but with opposite sign. This sign change in temperature across the tropopause, together with the spatially coherent ozone signatures, is consistent with extratropical potential vorticity anomalies remotely forced by tropical heating [e.g., *Hoskins et al.*, 1985, Figure 15]. We note that these ENSO-related ozone variations are as large or larger than those associated with the QBO (compare Figures 10 and 14), although they are significantly more localized in space than the QBO signals.

The residual ozone and temperature fluctuations analyzed here show overall strong coherence in middle and high latitudes but low correlations in the tropics, both for zonal mean and zonal wave components. Examination of the zonal mean residuals (Figure 15) allows identification of time periods which contribute to the low zonal mean correlations in the tropics, namely (1) slightly different ozone-temperature phasing during westerly acceleration phases of the QBO and (2) the warm temperature-low ozone signatures attributable to El Chichon and Pinatubo. The high correlation in extratropics for these month-to-month variations is likely due to dynamical coupling (see below).

As discussed in section 1, strong correlations between total ozone and lower stratospheric temperatures are expected due to both dynamical and radiative processes, with the latter becoming important for timescales long compared to the radiative relaxation time in the lower stratosphere (> 50-100 days). These two processes may be distinguished by their respective ratios of (ozone

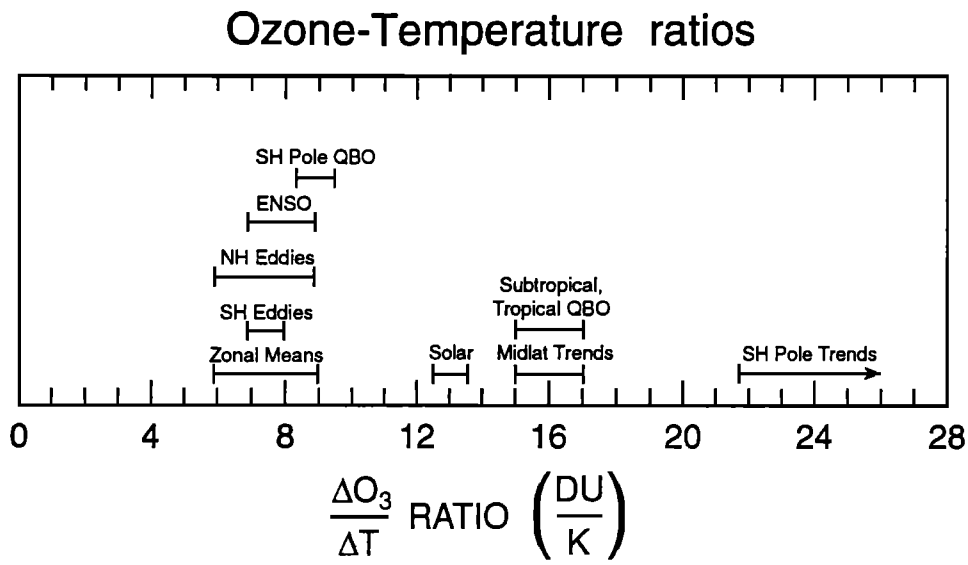

Figure 21. Plot of ozone-temperature ratios for the individual signals analyzed in this work, calculated as discussed in text.

change/temperature change). For dynamical variations the calculations of *Newman and Randel* [1988], *Tung and Yang* [1988], and *Wirth* [1993] give values in the range 6-10 DU/K. Results for the radiative effects are less certain, because a systematic analysis has not been published, and also the results depend on the assumed change in ozone profile [*Schwarzkopf and Ramaswamy*, 1993]. *Shine* [1986] and *Kiehl et al.* [1988] calculated the radiative response to an imposed Antarctic ozone hole, both giving ratios close to 16 DU/K. Estimates from the results of *Miller et al.* [1992], based on NH midlatitude calculations, are of the order of 15-20 DU/K (with significant uncertainties). These limited analyses suggest there may be a factor of 2 difference between the dynamically versus the radiatively determined ozone-temperature ratios.

Figure 21 shows the range of (ozone/temperature) ratios observed for the various signals discussed in this paper. These ratios are calculated from the regression-derived latitude-time diagrams simply as the ratio of ozone to temperature signals over regions where both signals are statistically significant; for example, the NH winter midlatitude trends in Figure 5 give a ratio of (-2.5 DU/yr)/(-0.15 K/yr) ≈ 17 DU/K. The ratios for the residual signals are calculated from regression analyses, over latitudes where the respective residual correlations are highest (from Figures 16-18).

The results summarized in Figure 21 show that the midlatitude trend, tropical and subtropical QBO, and solar signals all exhibit ozone-temperature ratios in the range 12-18 DU/K. Trend ratios over SH polar latitudes in October-November are somewhat larger (22-30 DU/K), although these ratios are more difficult to quantify from Figure 5 because the ozone and temperature trends show different temporal evolutions. The above ratios of 12-18 DU/K are in reasonable agreement with the radiatively determined ratios of 15-20 DU/K discussed above, suggesting that radiative effects are indeed important for these long time scale variations. Figure 21 furthermore shows a distinct separation between these ratios and those calculated for both the zonal mean and the wave residuals, which are in the range 6-9 DU/K. These smaller ratios are in excellent agreement with the dynamically based values quoted above. These data thus support the conclusion that the month-to-month residuals are coherent due to dynamical relationships, while radiative coupling is important for the longer timescales. One surprising result is that the ENSO- related ratios fall clearly within the dynamical regime (7-9 DU/K), although ENSO variations have timescales of the order of a year (Figure 2). The observed dynamical ratio might possibly be due to the strong seasonality observed in the ENSO signal, such that the appropriate timescales are seasonal rather than annual. We note also that the QBO ozone-temperature ratio over the SH pole in October-December falls in the dynamical regime (9 DU/K), and this may also possibly be related to strong seasonal coupling (although this argument does not apply to the subtropical QBO maxima, which are also seasonally synchronized).

Overall, there is reasonable agreement between the ratios derived empirically from the data here and those calculated theoretically. This gives us confidence in separating the results according to radiatively balanced longer timescale variations (trend, solar, and QBO) versus dynamically driven shorter ones (month-to-month residuals in particular). These results suggest that ozone radiative feedbacks are important for quantitative understanding of low-frequency variability in the stratosphere.

Acknowledgments. We acknowledge helpful discussions with Lane Bishop, Peter Bloomfield, Kunihiko Kodera, Masato Shiotani, Anne Smith, David Erickson, John Stanford, and Jerry Ziemke and for careful reviews by Tim Dunkerton, Rolando Garcia, and Roland Madden. Jim Hurrell provided easy access to the MSU data at NCAR, and Dennis Shea provided the reference time series in Figure 2. The manuscript was expertly prepared by Marilena Stone. Janel Cobb was supported by the undergraduate summer employment program at NCAR. This work has been supported under NASA grant W-16215. After completion of this manucript, we became aware of similar diagnostic analyses of TOMS data by C. Zerefos, K. Tourpali, and A. Bais (manuscript in preparation, 1994).

References

Angel, J. K., Variations and trends in tropospheric and stratospheric global temperatures, 1958-87, *J. Clim.*, *1*, 1296-1313, 1988.

Angel, J. K., On the relation between atmospheric ozone and sunspot number, *J. Clim.*, *2*, 1404-1416, 1989.

Angel, J. K., and J. Korshover, Quasi-biennial variations in temperature, total ozone, and tropopause height, *J. Atmos. Sci.*, *21*, 479-492, 1964.

Blackmon, M. L., J. E. Geisler, and E. J. Pitcher, A general circulation model study of January climate anomaly patterns associated with interannual variation of equatorial Pacific sea surface temperatures, *J. Atmos. Sci., 40*, 1410-1425, 1983.

Bowman, K. P., Global patterns of the quasi-biennial oscillation in total ozone, *J. Atmos. Sci., 46*, 3328-3343, 1989.

Brasseur, G., and C. Granier, Mount Pinatubo aerosols, chlorofluorocarbons, and ozone depletion, *Science, 257*, 1239-1242, 1992.

Chandra, S., Changes in stratospheric ozone and temperature due to the eruption of Mt. Pinatubo, *Geophys. Res. Lett., 20*, 33-36, 1993.

Chandra, S., and R. S. Stolarski, Recent trends in stratospheric total ozone: Implications of dynamical and El Chichon perturbations, *Geophys. Res. Lett., 18*, 2277-2280, 1991.

Dunkerton, T. J., and M. P. Baldwin, Modes of interannual variability in the stratosphere, *Geophys. Res. Lett., 19*, 49-52, 1992.

Dunkerton, T. J., and D. P. Delisi, Climatology of the equatorial lower stratosphere, *J. Atmos. Sci., 42*, 376-396, 1985.

Gao, X. H., and J. L. Stanford, Low-frequency oscillations in total ozone measurements, *J. Geophys. Res., 95*, 13,797-13,806, 1990.

Garcia, R. R., and S. Solomon, A possible relationship between interannual variability in Antarctic ozone and the quasi-biennial oscillation, *Geophys. Res. Lett., 14*, 848-851, 1987.

Gleason, J. F., et al., Record low global ozone in 1992, *Science, 260*, 523-526, 1993.

Gray, L. T., and T. J. Dunkerton, The role of the seasonal cycle in the quasi-biennial oscillation in ozone, *J. Atmos. Sci., 47*, 2429-2451, 1990.

Gray, L. T., and S. Ruth, The modeled latitudinal distribution of the ozone quasi-biennial oscillation using observed equatorial winds, *J. Atmos. Sci., 50*, 1033-1046, 1993.

Hamilton, K., Interhemispheric asymmetry and annual synchronization of the ozone quasi-biennial oscillation, *J. Atmos. Sci., 46*, 1019-1025, 1989.

Hasebe, F., A global analysis of the fluctuations in total ozone, II, Non-stationary annual oscillation, quasi-biennial oscillation, and long-term variations in total ozone, *J. Meteorol.. Soc. Jpn., 58*, 104-117, 1980.

Hasebe, F., Quasi-biennial oscillations of ozone and diabatic circulation in the equatorial stratosphere, *J. Atmos. Sci.*, in press, 1994.

Hofmann, D. J., and S. Solomon, Ozone destruction through heterogeneous chemistry following the eruption of El Chichon, *J. Geophys. Res., 94*, 5029-5041, 1989.

Holton, J. R., and H.-C. Tan, The influence of the equatorial quasi-biennial oscillation on the global circulation at 50 mb, *J. Atmos. Sci., 37*, 2200-2208, 1980.

Hood, L. L., and J. P. McCormack, Components of interannual ozone change based on Nimbus 7 TOMS data, *Geophys. Res. Lett., 19*, 2309-2312, 1992.

Horel, J. D., and J. M. Wallace, Planetary scale atmospheric phenomena associated with the southern oscillation, *Mon. Weather Rev., 109*, 813-829, 1981.

Hoskins, B. J., M. E. McIntyre, and A. W. Robertson, On the use and significance of isentropic potential vorticity maps, *Q. J. R. Meteorol. Soc., 111*, 877-946, 1985.

Karoly, D. J., Northern Hemisphere temperature trends: A possible greenhouse gas effect?, *Geophys. Res. Lett., 16*, 465-468, 1989.

Karoly, D. J., J. A. Cohen, G. A. Meehl, J.F.B. Mitchell, A. H. Oort, R. J. Stouffer, and R. T. Wetherald, An example of fingerprint detection of greenhouse climate change, *Clim. Dyn.*, in press, 1994.

Kiehl, J. T., B. A. Boville and B. P. Briegleb, Response of a general circulation model to a prescribed Antarctic ozone hole, *Nature , 332*, 501-504, 1988.

Kodera, K., The solar and equatorial QBO influences on the stratospheric circulation during the early Northern Hemisphere winter, *Geophys. Res. Lett., 18*, 1023-1026, 1991.

Kodera, K., and K. Yamazaki, Long-term variation of upper stratospheric circulation in the Northern Hemisphere in December, *J. Meteorol.. Soc. Jpn., 68*, 101-105, 1990.

Labitzke, K., and M. P. McCormick, Stratospheric temperature increases due to Pinatubo aerosols, *Geophys. Res. Lett., 19*, 207-210, 1992.

Labitzke, K., and H. van Loon, The spatial distribution of the association between total ozone and the 11-year solar cycle, *Geophys. Res. Lett., 19*, 401-403, 1992.

Labitzke, K., B. Naujokaf, and M. P. McCormick, Temperature effects on the stratosphere of the April 4, 1982 eruption of El Chichon, Mexico, *Geophys. Res. Lett., 10*, 24-26, 1983.

Lait, L. R., M. R. Schoeberl and P. A. Newman, Quasi-biennial modulation of the Antarctic ozone depletion, *J. Geophys. Res., 94*, 11559-11571, 1989.

McCormick, M. P., and T. J. Swissler, Stratospheric aerosol mass and latitudinal distribution of the El Chichon eruption cloud for October 1982, *Geophys. Res. Lett., 10*, 877-880, 1983.

McCormick, M. P., and R. E. Veiga, SAGE II measurements of early Pinatubo aerosols, *Geophys. Res. Lett., 19*, 155-158, 1992.

Meehl, G. A., and B. A. Albrect, Response of a GCM with a hybrid convective scheme to a tropical Pacific sea surface temperature anomaly, *J. Clim., 4*, 672-688, 1991.

Miller, A. J., R. M. Nagatani, G. C. Tiao, X. F. Niu, G. C. Reinsel, D. Wuebbles, and K. Grant, Comparisons of observed ozone and temperature trends in the lower stratosphere, *Geophys. Res. Lett., 19*, 929-932, 1992.

Mote, P. W., J. R. Holton, and J. M. Wallace, Variability in total ozone associated with baroclinic waves, *J. Atmos. Sci., 48*, 1900-1903, 1991.

Neter, J., W. Wasserman, and M. H. Kunter, *Applied Linear Statistical Models*, 1127 pp., 2nd edition, Richard D. Irwin, Homewood, Illinois, 1985

Newman, P. A., and W. J. Randel, Coherent ozone-dynamical changes during the southern hemisphere spring, 1979-1986, J. *Geophys. Res., 93*, 12,585-12,606, 1988.

Niu, X., J. E. Frederick, M. L. Stein, and G. C. Tiao, Trends in column ozone based on TOMS data: Dependence on month, latitude, and longitude, *J. Geophys. Res., 97*, 14,661-14,669, 1992.

O'Sullivan, D., and R. E. Young, Modeling the quasi-biennial oscillation's effect on the winter stratospheric circulation, *J. Atmos. Sci., 49*, 2437-2448, 1992.

Pan, Y.-H., and A. H. Oort, Global climate variations connnected with sea surface temperature anomalies in the eastern equatorial Pacific Ocean for the 1958-1973 period, *Mon. Weather Rev., 111*, 1244-1258, 1983.

Schoeberl, M. R., and A. J. Krueger, Medium scale disturbances in total ozone during Southern Hemisphere summer, *Bull. Am. Meteorol. Soc., 64*, 1358-1365, 1983.

Schoeberl, M. R., P. K. Bhartia, and E. Hilsenrath, Tropical ozone loss following the eruption of Mt. Pinatubo, *Geophys. Res. Lett., 20*, 29-32, 1993.

Schwarzkopf, M. D., and V. Ramaswamy, Radiative forcing due to ozone in the 1980s: Dependence on altitude of ozone change, *Geophys. Res. Lett., 20*, 205-208, 1993.

Shine, K. P., On the modeled thermal response of the Antarctic stratosphere to a depletion of ozone, *Geophys. Res. Lett., 13*, 1331-1334, 1986.

Shiotani, M., Annual, quasi-biennial, and El Niño-Southern Oscillation (ENSO) timescale variations in equatorial total ozone, *J. Geophys. Res., 97*, 7625-7633, 1992.

Spencer, R. W., and J. R. Christy, Precision lower stratospheric temperature monitoring with the MSU: Technique, validation and results 1979-1991, *J. Clim., 6*, 1194-1204, 1993.

Stolarski, R. S., P. Bloomfield, R. D. McPeters, and J. R. Herman, Total ozone trends deduced from Nimus 7 TOMS data, *Geophys. Res. Lett., 18*, 1015-1018, 1991.

Stolarski, R., R. Bojkov, L. Bishop, C. Zerefos, J. Staehelin, and J. Zawodny, Measured trends in stratospheric ozone, *Science, 256*, 342-349, 1992.

Trenberth, K. E., Recent observed interdecadal climate change in the Northern Hemisphere, *Bull. Am. Meteorol. Soc., 71*, 988-993, 1990.

Tung, K. K., and H. Yang, Dynamic variability of column ozone, *J. Geophys. Res., 93*, 11123-11128, 1988.

van Loon, H., and K. Labitzke, Association between the 11-year solar cycle and the atmosphere, IV, The stratosphere, not grouped by the phase of the QBO, *J. Clim., 3*, 827-837, 1990.

Wirth, V., Quasi-stationary planetary waves in total ozone and their correlation with lower stratospheric temperature, *J. Geophys. Res.*, *98*, 8,873-8,882, 1993.

World Meteorological Organization (WMO), Report of the international ozone trends panel—1988, *WMO Rep. 18*, Geneva, 1988.

Yulaeva, E., and J. M. Wallace, The signature of ENSO in global temperature fields derived from the microwave sounding unit, *J. Clim.*, in press, 1994.

Zerefos, C. S., A. F. Bais, I. C. Ziomas, and R. D. Bojkov, On the relative importance of quasi-biennial oscillation and El Niño/Southern Oscillation in the revised Dobson total ozone records, *J. Geophys. Res.*, *97*, 10,135-10,144, 1992.

J. B. Cobb and W. J. Randel, National Center for Atmospheric Research, Division of Atmospheric Chemistry , P. O. Box 3000, Boulder, CO 80307.

(Received May 21, 1993; revised November 10, 1993;
accepted November 29, 1993.